International Journal of Thermophysics, Vol. 24, No. 4, July 2003 (© 2003)

Thermophysical Property Measurements of Supercooled and Liquid Rhodium

P.-F. Paradis,[1,2] T. Ishikawa,[1] and S. Yoda[1]

Received January 23, 2003

The density, the isobaric heat capacity, the surface tension, and the viscosity of liquid rhodium were measured over wide temperature ranges, including the supercooled phase, using an electrostatic levitation furnace. Over the 1820 to 2250 K temperature span, the density can be expressed as $\rho(T) = 10.82 \times 10^3 - 0.76(T - T_m)$ $(kg \cdot m^{-3})$ with $T_m = 2236$ K, yielding a volume expansion coefficient $\alpha(T) = 7.0 \times 10^{-5}$ (K^{-1}). The isobaric heat capacity can be estimated as $C_P(T) = 32.2 + 1.4 \times 10^{-3}(T - T_m)$ $(J \cdot mol^{-1} \cdot K^{-1})$ if the hemispherical total emissivity of the liquid remains constant at 0.18 over the 1820 to 2250 K interval. The enthalpy and entropy of fusion have also been measured, respectively, as 23.0 $kJ \cdot mol^{-1}$ and 10.3 $J \cdot mol^{-1} \cdot K^{-1}$. In addition, the surface tension can be expressed as $\sigma(T) = 1.94 \times 10^3 - 0.30(T - T_m)$ $(mN \cdot m^{-1})$ and the viscosity as $\eta(T) = 0.09 \exp[6.4 \times 10^4 (RT)]$ $(mPa \cdot s)$ over the 1860 to 2380 K temperature range.

KEY WORDS: density; heat capacity; enthalpy of fusion; entropy of fusion; liquid metal; rhodium; supercooling; surface tension; viscosity.

1. INTRODUCTION

Rhodium has been employed in furnace windings, thermocouple elements, electrodes for aircraft spark plugs, and laboratory crucibles due to its refractory nature, its resistance to corrosion, and its ability to be successfully alloyed with platinum and palladium. In addition, its low electrical resistance makes it attractive as an electrical contact material. However, its high melting temperature (2236 ± 3 K) and its reactivity with oxygen at elevated temperature [1], make the measurement of its thermophysical

[1] National Space Development Agency of Japan, Tsukuba Space Center, 2-1-1 Sengen, Tsukuba, Ibaraki 305-8505, Japan.

[2] To whom correspondence should be addressed. E-mail: paradis.paulfrancois@nasda.go.jp

0195-928X/03/0700-1121/0 © 2003 Plenum Publishing Corporation

properties challenging above the melting temperature and under deep supercooled conditions using traditional methods. A knowledge of the thermophysical properties and their temperature dependences is important for studies on phase transformations, nucleation, atomic dynamics, and surface physics, as well as for industrial processes (e.g., refining, casting, and welding). These properties are also useful when designing alloys because the properties of an end member (e.g., binary and ternary systems) are required to estimate those of the final alloy.

In this study, an electrostatic levitation furnace developed by the National Space Development Agency of Japan (NASDA) [2, 3] overcame the problems associated with high temperature processing and could be used for accurate determination of the thermophysical properties. Measurements were achieved in vacuum by using multiple laser heating beams to isolate the sample from contaminating walls as well as surrounding gases and to provide adequate position stability [4]. Containerless conditions and no heat input from the levitation scheme permitted deep supercooling of the sample.

This paper first describes the facility and the thermophysical property measurement methods and then presents the experimental results. In this work, several properties of liquid and supercooled rhodium (density, thermal expansion coefficient, isobaric heat capacity, surface tension, viscosity) were determined and the values of the enthalpy and entropy of fusion were calculated.

2. EXPERIMENTAL SETUP AND PROCEDURES

2.1. Electrostatic Levitation Furnace

The measurements were made using an electrostatic levitator based on a design by Rhim et al. [5] but with several modifications (levitation initiation, charging, handling, imaging, heating configuration) without which the experiments would have been very challenging [2–4, 6]. The facility (Fig. 1a), described earlier [2, 3, 7], consisted of a chamber that was evacuated to $\sim 10^{-5}$ Pa before processing was initiated. The chamber housed a sample charged by electronic emission and levitated between two disk electrodes, 10 mm apart. These electrodes were used to control the sample in the vertical position (z) via a feedback loop (Fig. 1b). Four spherical electrodes distributed around the bottom electrode were used for horizontal control (x, y). The positioning control relied on two sets of orthogonally disposed He-Ne lasers and the associated position detectors. The sample position information was fed to a computer that inputs new values of x, y, z to a high voltage amplifier so that a prefixed position could be

maintained. The lower electrode was surrounded by four coils that generated a rotating magnetic field that was used for rotation control [8]. To excite drop oscillations, an ac voltage was superimposed on the levitation voltage from the bottom electrode (Fig. 1a) [9]. Specimens were prepared by arc melting 99.9 mass% purity rhodium powder (Nilaco Corporation, Tokyo, Japan) into spheroids with diameters of ca. 2 mm.

Two 100 W CO_2 lasers (10.6 μm emission) were used for heating. One beam was sent directly to the sample whereas the other beam was divided into two portions such that three focused beams, separated by 120 degrees, hit the specimen. Computer control helped to ensure that each beam delivered equal power to the sample. Equal heating was important to minimize possible non-isotropic evaporation that could cause sample position instability. In addition, this configuration, along with controlled sample rotation (< 5 Hz), provided temperature homogeneity. Two pyrometers,

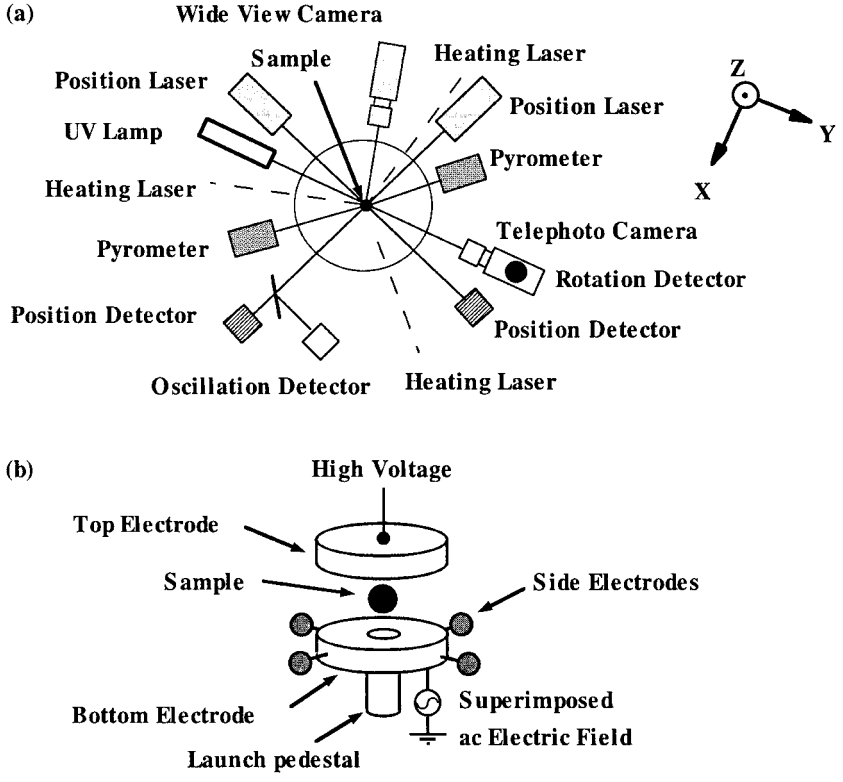

Fig. 1. Schematic views: (a) electrostatic levitation furnace and (b) electrode assembly.

operating, respectively, at 0.90 μm and 0.96 μm (acquisition rates of 10 and 120 Hz) and covering a 1070 to 3800 K interval, were used as two single wavelength pyrometers for temperature recording.

The sample was observed by two charged-coupled-device (CCD) cameras located at 90 degrees with respect to each other. This helped to monitor the sample position in the horizontal plane and to align the heating laser beams to minimize any photon induced rotation or oscillation on the sample [10]. One camera offered a view of both the electrodes and the sample whereas a second black and white high-resolution camera equipped with a telephoto objective in conjunction with a background light provided a magnified view of the sample. A half-mirror, an interference filter (He-Ne emission line), and a sensor, allowing the sample rotation rate to be measured by detecting the reflected He-Ne laser beam from its surface, were attached to the telephoto objective [8]. Control of rotation was important while measuring the density, surface tension, and viscosity since a sample deformed by rotation could lead to erroneous data [8]. Another detector, coupled with a monochromator slit, was dedicated to the measurement of the sample oscillation, from which the surface tension and viscosity could be determined [10].

2.2. Thermophysical Properties Determination

Before the properties were measured, a spheroid sample was first melted and re-solidified to confirm pyrometer calibration and alignment and to ensure that the sample, prepared by arc-melting, was spherical. If the shape of a liquefied sample departed from that of a sphere during processing (due to excessive rotation), a counter torque was applied either with a magnetic field [8] or by appropriately steering the beams of the heating lasers [10] to restore the spherical shape. Sphericity was confirmed by software analysis by comparing the sample shape with that of a calibration sphere.

The techniques used to determine the density and the ratio of constant pressure heat capacity over hemispherical total emissivity (C_P/ε_T) have been described in the literature and are summarized below [11, 12]. Once the sample was melted, it took a spherical shape due to surface tension and the distribution of surface charge. Also, since electrostatic levitation did not input any heat, a molten sample experienced pure radiative cooling when the heating laser beams were blocked and the resulting energy equation governing the cooling process reduced to

$$(mC_P/M)\, dT/dt = -\varepsilon_T A\sigma(T^4 - T_{amb}^4) \tag{1}$$

where m is the sample mass, M is the molar mass, C_P is the isobaric molar heat capacity, ε_T is the hemispherical total emissivity, A is the sample area, σ is the Stefan-Boltzmann constant, and T and T_{amb} are, respectively, the sample and ambient temperatures. The radiance temperature was measured by the pyrometers and was calibrated to the true temperature using the known melting temperature of the sample ($T_m = 2236\,K$) at the melting plateau. Calibration to the true temperature was performed using custom-made Code Warrior™ software. A typical temperature profile for a cooling rhodium sample exhibiting 415 K supercooling and recalescence (sudden temperature rise due to the release of the latent heat of fusion of an undercooled sample upon solidification), is shown in Fig. 2. The change in the slope shortly after recalescence could possibly be explained by a change in the emissivity of the high temperature solid sample. No emissivity corrections were made for the solid part of the curve. After the sample started to cool, both the image and the cooling curve data could be used to measure simultaneously the density and the ratio of the isobaric heat capacity and hemispherical total emissivity.

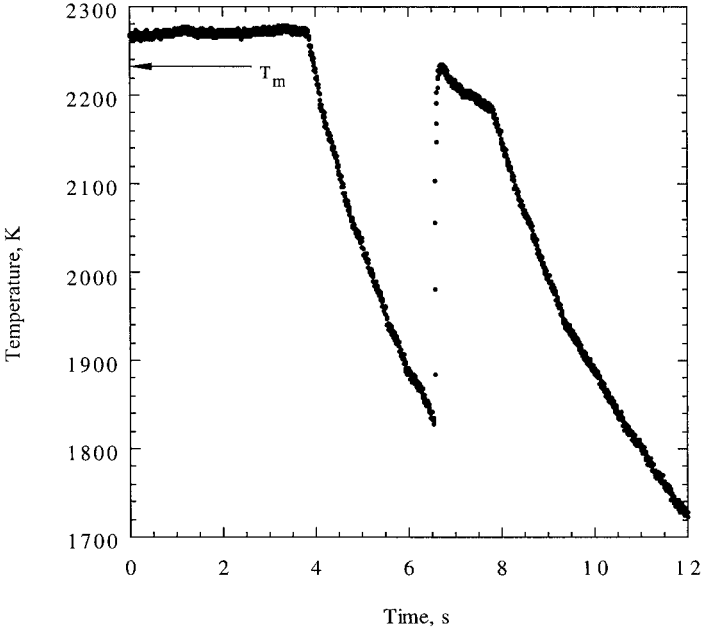

Fig. 2. Radiative cooling curve for rhodium showing supercooling and recalescence (sudden temperature rise due to the release of the latent heat of fusion of an undercooled sample upon solidification).

Sample imaging was achieved by the high-resolution camera (Sony SSC-M370) equipped with a high-pass filter (450 nm), in conjunction with a high intensity UV background lamp. This gave a close look at the sample, allowing the perimeter to be analyzed. The use of the UV lamp offered a background lighting efficiency that was practically independent of sample temperature (from well above T_m down to the supercooled state), yielding excellent imaging, thus providing an accurate determination of both density and the ratio of the isobaric heat capacity and the hemispherical total emissivity [6]. For density measurements, the recorded images were digitized and matched to the cooling curve. A program then extracted the area from each image. Since the sample was axi-symmetric and because its mass was known, the density could be found for each temperature. The ratio of the isobaric heat capacity and hemispherical total emissivity could be found from Eq. (1) since all parameters were known, and since the area was found from the images and dT/dt from the cooling curve.

The surface tension and viscosity were determined by measuring the frequency of the sample oscillation about its equilibrium shape [13, 14]. This method, described elsewhere [10] and explained below for completeness, allowed measurements of supercooled and highly reactive melts. To measure the surface tension using this method, a sample was first heated, melted, and brought to a selected temperature. Then, a $P_2\cos(\theta)$-mode drop oscillation was induced to the sample by superimposing a small sinusoidal electric field on the levitation field. The transient signal that followed the termination of the excitation field was detected and analyzed using an in-house LabVIEW™ program. At the melting temperature, the frequency of the drop oscillation was around 200 Hz and the amplitude was about 1.1 times the sample radius. This was done several times at a given temperature and repeated for numerous temperatures. Using the characteristic oscillation frequency ω_c of this signal after correcting for nonuniform surface charge distribution [15], the surface tension σ can be found from [9]

$$\omega_c^2 = (8\sigma/r_0^3\rho)[1-(Q^2/64\pi^2 r_0^3\sigma\varepsilon_0)][1-F(\sigma, q, e)] \tag{2}$$

where

$$F(\sigma, q, e) = [243.31\sigma^2 - 63.14q^2\sigma + 1.54q^4]\, e^2/[176\sigma^3 - 120q^2\sigma^2 + 27\sigma q^4 - 2q^6], \tag{3}$$

r_0 is the radius of the sample when it assumes a spherical shape, ρ is the liquid density, Q is the drop charge, determined from electrode spacing

and applied field [5], ε_0 is the permittivity of vacuum, and q and e are defined by

$$q^2 = Q^2/(16\pi^2 r_0^3 \varepsilon_0) \tag{4}$$

and

$$e^2 = E^2 r_0 \varepsilon_0 \tag{5}$$

respectively, with E being the applied electric field. Similarly, using the decay time τ given by the same signal, the viscosity η was found by

$$\eta = \rho r_0^2/(5\tau). \tag{6}$$

Equations (2) and (6) imply that both the surface tension and the viscosity depend on the sample radius and density. For density, we simply substituted our previously determined data in these equations. Furthermore, image analysis was simultaneously used for radius measurements to prevent any distortion in the measured properties due to sample evaporation.

3. EXPERIMENTAL RESULTS

3.1. Density

The density measurements of liquid rhodium, taken over the 1820 to 2250 K temperature range and covering the supercooled region by nearly 420 K, are shown in Fig. 3. The density, like that of other pure metals, exhibited a linear behavior as a function of temperature and can be fitted by the relationship:

$$\rho(T) = 10.82 \times 10^3 - 0.76(T - T_m)\ (\mathrm{kg \cdot m^{-3}}) \qquad (1820 \text{ to } 2250\ \mathrm{K}) \tag{7}$$

where T_m is the melting temperature (2236 K). In these measurements, the uncertainty was estimated to be less than 2 per cent from the resolution of the video grabbing capability (640×480 pixels) and from the uncertainty in mass measurement (± 0.0001 g). To our knowledge, these measurements were the first to be reported that covered such a large temperature span into the supercooled region. The values that appeared in the literature are summarized in Table I for comparison. At the melting temperature, our value is 2.5% smaller compared with that calculated by Allen [16] from room-temperature specific volumes increased by an allowance for the cubical thermal expansion to the melting point and an estimated amount for fusion. It agrees, within experimental uncertainties, with that calculated

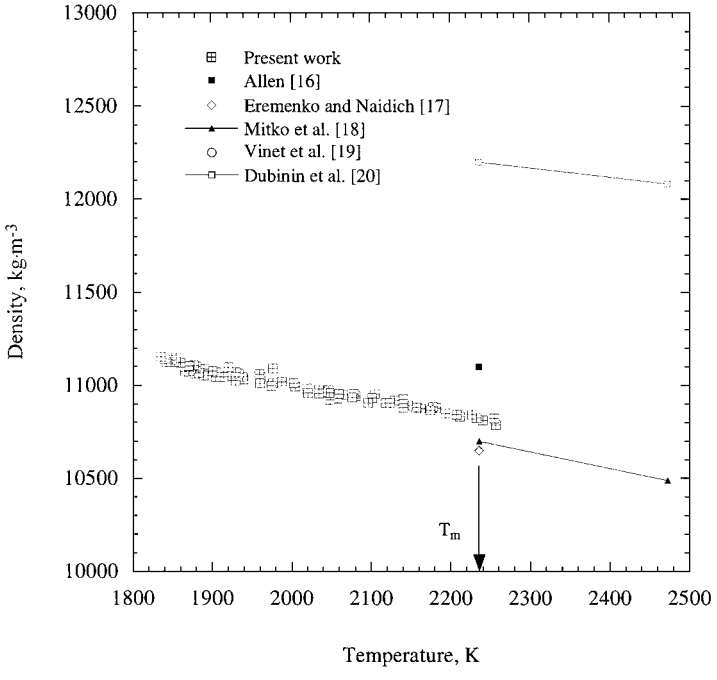

Fig. 3. Density of rhodium versus temperature.

by Eremenko and Naidich [17] and those measured by Mitko et al. [18] with the sessile drop technique in helium and by Vinet et al. [19] with the pendant drop method. It is, however, 11.3% smaller than that obtained by Dubinin et al. [20] with the sessile drop technique in vacuum. Our temperature coefficient was nearly 15% lower than that obtained by Mitko et al. [18] and 1.5 times larger compared with that of Dubinin et al. [20].

Table I. Comparisons with Literature Values of the Density of Rhodium

Density@T_m (10^3 kg·m^{-3})	Temperature Coeff. (kg·m^{-3}·K^{-1})	Temperature (K)	Reference	Technique
10.82	−0.76	1820–2250	present work	levitation
11.1	–	2236	Allen [16]	calculated
10.65	–	2236	Eremenko and Naidich [17]	calculated
10.7	−0.8955	2236–2473	Mitko et al. [18]	sessile drop (He)
10.7	–	2236	Vinet et al. [19]	pendant drop
12.20	−0.50	2236–2473	Dubinin et al. [20]	sessile drop (vac)

The volume variation $V(T)$ of the molten state, normalized with the volume at the melting temperature V_m, was derived from Eq. (7), and can be expressed by

$$V(T)/V_m = 1 + 7.0 \times 10^{-5}(T - T_m) \qquad (1820 \text{ to } 2250 \text{ K}) \qquad (8)$$

where 7.0×10^{-5} represents the volume expansion coefficient $\alpha(T)$.

The discrepancy between our results and those of Mitko et al. [18] and Dubinin et al. [20] could be attributed to the difference in processing techniques and the extent to which evaporation losses have been considered. We used a containerless approach in high vacuum that isolated our samples from container walls and gases and took into account evaporation in determining the final density values.

3.2. Isobaric Heat Capacity

The ratio between the isobaric heat capacity and the hemispherical total emissivity as a function of the temperature is shown in Fig. 4 for

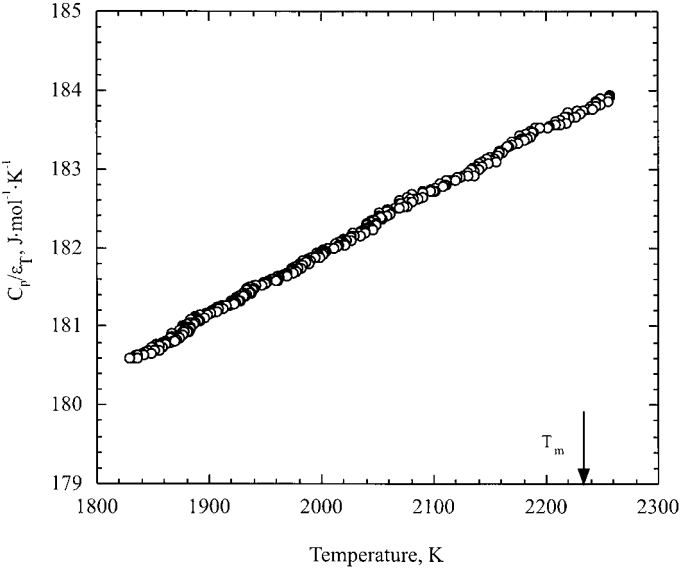

Fig. 4. Ratio between the isobaric heat capacity and the hemispherical total emissivity of rhodium versus temperature.

liquid rhodium. The $C_P(T)/\varepsilon_T(T)$ is nearly constant with temperature and can be linearly fitted as

$$C_P(T)/\varepsilon_T(T) = 184.0 + 8.0 \times 10^{-3}(T - T_m)\ (\mathrm{J \cdot mol^{-1} \cdot K^{-1}}) \quad (1820 \text{ to } 2250\ \mathrm{K}). \tag{9}$$

The value of ε_T, found from the pyrometer setting at the melting temperature, was equal to 0.18. Although recent measurements with a fast polarimeter did show variations in the emissivity in the liquid phase of several metals [21], the lack of data for liquid and supercooled rhodium prompted us to assume that $\varepsilon_T(T)$ remained constant over the whole temperature range. The temperature dependence of $C_P(T)$ would then be determined from Eq. (9) by simply multiplying it by $\varepsilon_T(T) = 0.18$. The heat capacity so obtained (Fig. 5) can be expressed as

$$C_P(T) = 32.2 + 1.4 \times 10^{-3}(T - T_m)\ (\mathrm{J \cdot mol^{-1} \cdot K^{-1}}) \qquad (1820 \text{ to } 2250\ \mathrm{K}). \tag{10}$$

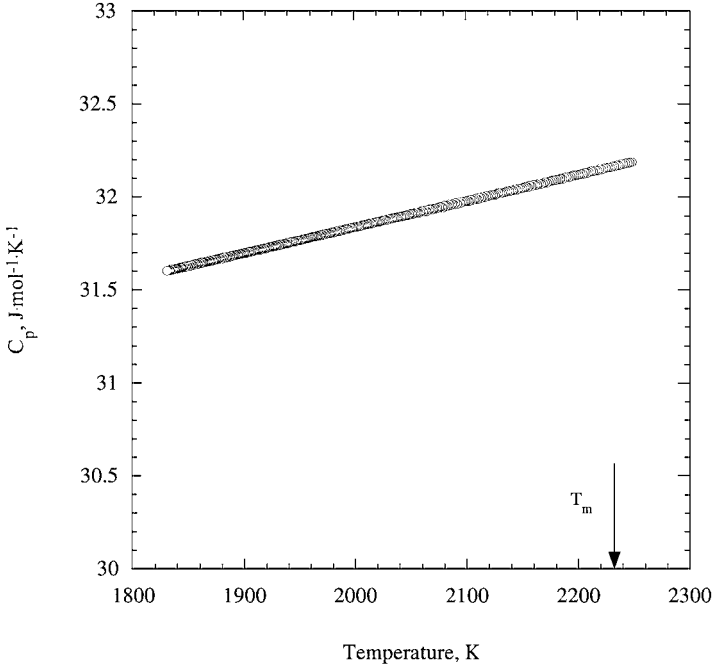

Fig. 5. Heat capacity of rhodium versus temperature, calculated using the data from Fig. 4 and $\varepsilon_T(T) = 0.18$.

Table II. Comparisons with Literature Values of the Enthalpy and Entropy of Fusion of Rhodium

Enthalpy of fusion ($kJ \cdot mol^{-1}$)	Entropy of fusion ($J \cdot mol^{-1} \cdot K^{-1}$)	Reference	Technique
23.0	10.3	present work	levitation
21.5	9.6	Barin et al. [22]	calculated

Adding the enthalpy contributions of the supercooled liquid and that of the isothermal region following recalescence (see Fig. 2), the latent heat of fusion has been determined. The contribution of the supercooled portion was found by integrating $C_P(T)$ over temperature from T_m to the lowest temperature of supercooling, whereas that of the isothermal solid was obtained by integrating $\varepsilon_{TS} A\sigma\ (T^4 - T_{amb}^4)$ over the averaged time at which the solid stays at T_m. The enthalpy of fusion ΔH was found to be equal to 23.0 $kJ \cdot mol^{-1}$ which allowed the entropy of fusion ΔS to be obtained from the relationship,

$$\Delta S = \Delta H / T_m \tag{11}$$

as 10.3 $J \cdot mol^{-1} \cdot K^{-1}$. These data are nearly 7% larger than the theoretical values reported by Barin et al. [22] (Table II). The differences could, in part, be attributed to the slow response of our pyrometer, which lags the recalescence phenomenon, thus inducing errors in time and uncertainties in $C_P(T)$ or ε_T.

3.3. Surface Tension

Figure 6 depicts our results for the surface tension. The surface tension of rhodium, as that of other pure metals, exhibited a linear relationship as a function of temperature. In this experiment, the uncertainty of the measurements was estimated to be better than 5 percent from the response of the oscillation detector and from the density measurements. The data available from the literature are also superimposed on the same figure for comparison. In addition, Table III summarizes the existing data with a corresponding temperature range of applicability and measurement technique. The surface tension (Fig. 6) measured over the 1860 to 2380 K temperature range and covering the undercooled region by 375 K, can be expressed by

$$\sigma(T) = 1.94 \times 10^3 - 0.30(T - T_m)\ (mN \cdot m^{-1}) \qquad (1860 \text{ to } 2380\ K) \tag{12}$$

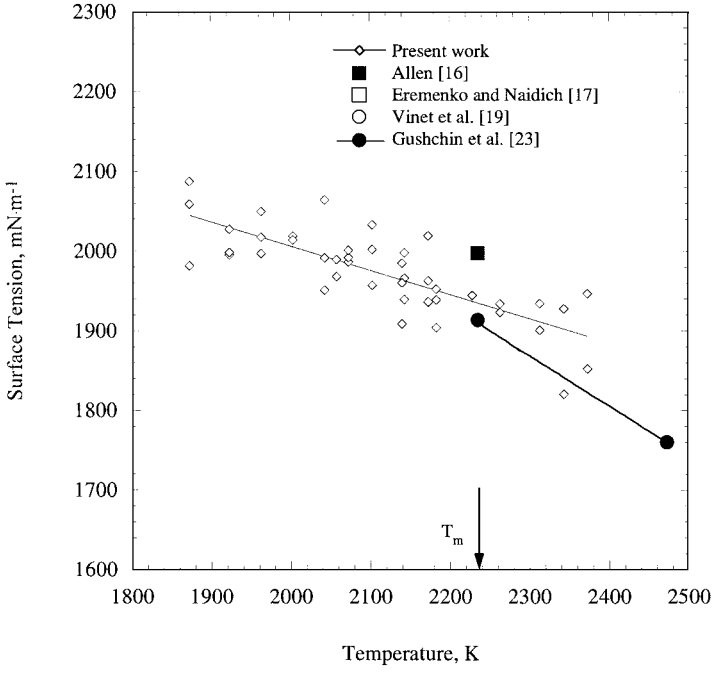

Fig. 6. Surface tension of rhodium versus temperature.

where T_m is the melting temperature. These measurements were the first to cover a large temperature interval in the supercooled region. At the melting temperature, our result is, within experimental uncertainties, in agreement with that obtained by Eremenko and Naidich [17] with the sessile drop in vacuum, with that measured by Vinet et al. [19] with the pendant drop method, and with that determined by Gushchin et al. [23] with the sessile drop in helium. It is over 3 percent smaller compared with that reported by

Table III. Comparisons with Literature Values of the Surface Tension of Rhodium

Surface Tension@T_m ($mN \cdot m^{-1}$)	Temperature Coeff. ($mN \cdot m^{-1} \cdot K^{-1}$)	Temperature (K)	Reference	Technique
1940	−0.303	1860–2380	present work	levitation
2000	–	2236	Allen [16]	pendant drop (vac)
1940	–	2236	Eremenko and Naidich [17]	sessile drop (vac)
1940	–	2236	Vinet et al. [19]	pendant drop
1915	−0.664	2236–2473	Gushchin et al. [23]	sessile drop (He)

Allen [16] using the pendant drop method. Our temperature coefficient is, however, less than half of that measured by Gushchin et al. [23].

The discrepancies between our results and those reported by the other investigators [16, 23] could stem from the differences in processing techniques. In this work, containerless levitation in high vacuum and radiative heating isolated the samples from container walls and gases, whereas the above authors employed the pendant drop or sessile drop methods for which possible chemical reactions between the highly reactive molten metal and a solid support could have occurred. In addition, electron bombardment and induction heating, used elsewhere, might have been accompanied with some evaporation from the electrodes or from the heating elements, thus further contaminating the specimen under study. This could have affected the surface tension, highly dependent upon contamination. In our experiments, no oxide or nitride patches were either tracked by the rotation detection or by visual observation when the rhodium sample was liquid (previous experiments with tin showed that oxide patches could be detected either visually or with the rotation detection system). The purity of the samples and the level of vacuum or the presence of an atmosphere could also explain the discrepancies between our data and those obtained by other investigators [16, 23].

3.4. Viscosity

By extracting the decay time component from the decay of the oscillation of a drop, it was possible to determine the viscosity of the liquid and supercooled rhodium over the 1860 to 2380 K range. Figure 7 illustrates our data, together with the datum obtained by Demidovich et al. with the capillary technique [24], the only value found in the literature. The data can be fitted by the following Arrhenius function:

$$\eta(T) = 0.09 \exp[6.4 \times 10^4/(RT)] \text{ (mPa} \cdot \text{s)} \qquad (1860 \text{ to } 2380 \text{ K}) \qquad (13)$$

where R, the gas constant, is equal to $8.31 \text{ J} \cdot \text{mol}^{-1} \cdot \text{K}^{-1}$. At the melting temperature, it is 1.5 times larger compared with that reported in Ref. 24 (Table IV). The discrepancy might be explained by the contamination generated by the capillary and also by the difference in specimen purities. In addition, the damping time and thus, the viscosity data, could also have been altered because the control software tries to restore any sample displacement. Since viscosity is a bulk property, the effects of charge should be very small, if any, and were therefore neglected. By comparison, the correction for charge for the surface tension of Rh (a surface property) was about 2% and was taken into account.

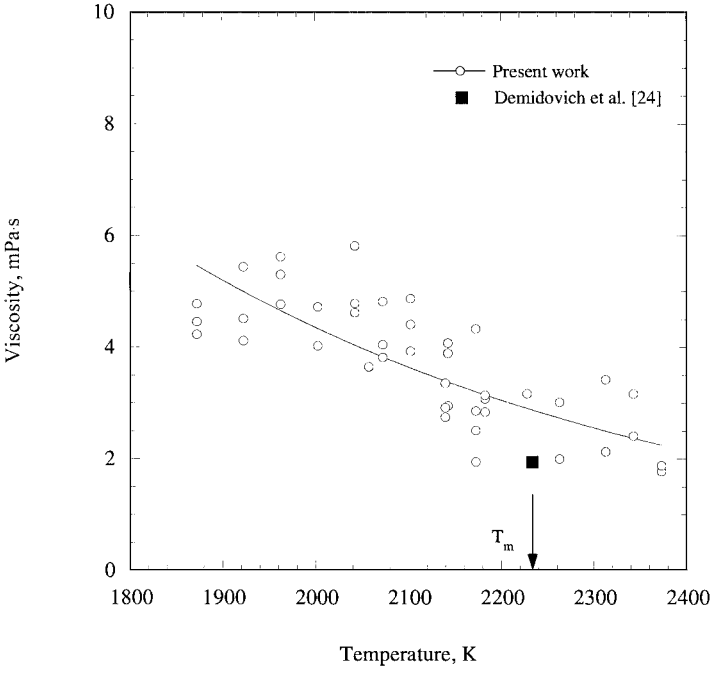

Fig. 7. Viscosity of rhodium versus temperature.

5. CONCLUSIONS

Numerous thermophysical properties of liquid rhodium measured with the NASDA electrostatic levitation furnace were presented. For the first time, the density of liquid rhodium is reported over a wide temperature range in the supercooled state. Also given in this paper are the thermal expansion coefficient, the enthalpy and entropy of fusion, and the ratio of the isobaric heat capacity to the hemispherical total emissivity of the liquid

Table IV. Comparisons with Literature Values of the Viscosity of Rhodium

Viscosity@T_m (mPa·s)	Temperature Dependence	Temperature (K)	Reference	Technique
2.867	0.09 exp[64319/(RT)]	1860–2380	present work	levitation
1.966	–	2236	Demidovich et al. [24]	capillary

phase. The surface tension and viscosity of rhodium over large temperature intervals, including the supercooled phase, are also reported for the first time.

Future efforts will be devoted to determine similar properties for liquid and supercooled tantalum, rhenium, and tungsten.

ACKNOWLEDGMENTS

We would like to express our deepest gratitude to the Japan Society for the Promotion of Science for their Grant-in-Aid for Scientific Research (B). Sincere thanks are also directed to Dr. J. Yu for his careful reading of the manuscript and to T. Saita (Advanced Engineering Services) and Dr. Aoyama for their help in the data-taking process.

REFERENCES

1. D. R. Lide and H. P. R. Frederikse, eds., *CRC Handbook of Chemistry and Physics*, 78th Ed. (CRC Press, Boca Raton, Florida, 1997).
2. P.-F. Paradis, T. Ishikawa, and S. Yoda, in *Proc. First Int. Symp. Microgravity Res. Applications in Phys. Sci. and Biotech.*, Sorrento, Italy, September 2000 (ESA SP-454) (2001), p. 993.
3. T. Ishikawa, P.-F. Paradis, and S. Yoda, *J. Jpn. Soc. Microg. Appl.* **18**:106 (2001).
4. P.-F. Paradis, T. Ishikawa, and S. Yoda, *Space Technol.* **22**:81 (2002).
5. W.-K. Rhim, S.-K. Chung, D. Barber, K.-F. Man, G. Gutt, A. A. Rulison, and R. E. Spjut, *Rev. Sci. Instrum.* **64**:2961 (1993).
6. T. Ishikawa, P.-F. Paradis, and S. Yoda, *Rev. Sci. Instrum.* **72**:2490 (2001).
7. P.-F. Paradis, T. Ishikawa, and S. Yoda, *Int. J. Thermophys.* **23**:825 (2002).
8. W.-K. Rhim and T. Ishikawa, *Rev. Sci. Instrum.* **69**:3628 (1998).
9. W.-K. Rhim, K. Ohsaka, P.-F. Paradis, and R. E. Spjut, *Rev. Sci. Instrum.* **70**:2796 (1999).
10. W.-K. Rhim and P.-F. Paradis, *Rev. Sci. Instrum.* **70**:4652 (1999).
11. S.-K. Chung, D. B. Thiessen, and W.-K. Rhim, *Rev. Sci. Instrum.* **67**:3175 (1996).
12. A. A. Rulison and W.-K. Rhim, *Rev. Sci. Instrum.* **65**:695 (1994).
13. Lord Rayleigh, *Proc. R. Soc. London.* **14**:184 (1882).
14. S. Sauerland, G. Lohofer, and I. Egry, *J. Non Cryst. Solids.* **156-158**:833 (1993).
15. J. Q. Feng and K. V. Beard, *Proc. R. Soc. London. A* **430**:133 (1990).
16. B. C. Allen, *Trans. AIME* **227**:1175 (1963).
17. V. N. Eremenko and E. J. Naidich, *Izv. Akad. Nauk., O.T.N.* **6**:100 (1961).
18. M. M. Mitko, E. L. Dubinin, A. I. Timofeev, and L. I. Chegodaev, *Izv. Vyss. Uchebn, Saved. Met. (SU)* **3**:84 (1978).
19. B. Vinet, L. Magnusson, H. Fredriksson, and J.-P. Desre, *J. Coll. Interf. Sci.* **255**:363 (2002).
20. E. L. Dubinin, V. M. Vlasov, A. I. Timofeev, S. O. Safonov, and A. I. Chegodaev, *Izv. Vyss. Uchebn. Saved., Tsvetn. Met.* **4**:160 (1975).
21. A. Seifter, C. Cagran, and G. Pottlacher, in *Proc. Sixth Euro. Conf. Thermophys. Prop.*, London, UK, September 2002 (ESA SP-454) (2001), p. 176.

22. I. Barin, O. Knacke, and O. Kubaschewski, *Thermochemical Properties of Inorganic Substances* (Springer-Verlag, Berlin, 1977) in *Condensed Matter–Disordered Solids*, S. K. Srivastava and N. H. March, eds. (World Scientific, Singapore, 1995).
23. S. G. Gushchin, N. A. Vatolin, E. L. Dubinin, and A. I. Timofeev, *Ogneupory (USSR)* **12**:49 (1977).
24. O. V. Demidovich, A. A. Zhuchenko, E. L. Dubinin, N. A. Vatolin, A. I. Timofeev, *Izv. Akad. Nauk. SSSR Met. (SU)* **1**:73 (1979).